

Supporting Information

Silicon Carbide as a Protective Layer to Stabilize Si-Based Anodes by Inhibiting Chemical Reactions

Chunhui Yu[‡], Xiao Chen[‡], Zhexi Xiao, Chao Lei, Chenxi Zhang, Xianqing Lin,

*Boyuan Shen, Rufan Zhang, and Fei Wei**

C. Yu, X. Chen, Z. Xiao, C. Lei, C. Zhang, X. Lin, B. Shen, R. Zhang, Prof. F. Wei

Beijing Key Laboratory of Green Chemical Reaction Engineering and Technology

Department of Chemical Engineering

Tsinghua University

Beijing 100084, China

*Email: wf-dce@tsinghua.edu.cn (F. Wei).

Calculation of the activation energy of the side reaction

The Arrhenius formula was used to describe the effect of nanocarbon. In the Arrhenius formula (eq. 1), k represents the reaction rate constant, A is the pre-exponential factor, T is the absolute temperature (in Kelvin), E_a is the activation energy of the reaction, R is the universal gas constant and $\ln k$ is proportional to $1/T$. Assuming that the side reaction is a first-order surface reaction, the conversion rate X is proportional to the reaction rate constant k (eq. 2). Therefore, $\ln X$ is proportional to $1/T$ (eq. 3). In the graph of $\ln X$ and $1/T$, the slope represents E_a/R . By changing the reaction temperature, a graph of $\ln X$ and $1/T$ allows the activation energy to be obtained. The activation energy of Si@C (38.98 kJ/mol) was only half that of Si (76.98 kJ/mol), indicating that nanocarbon acts as a catalyst to increase the reaction rate for Li_2SiF_6 aggregate formation.

$$\ln k = \ln k_0 - E_a/RT \quad (1)$$

$$X \propto k \quad (2)$$

$$\ln X \propto 1/T \quad (3)$$

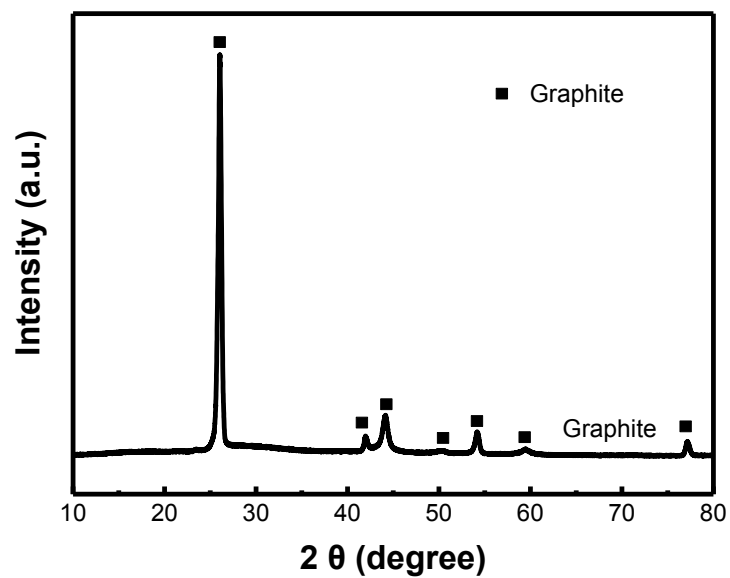


Figure S1. XRD data of graphite after the reaction.

The XRD data of graphite after the reaction showed no peaks for the Li_2SiF_6 crystal. This result proved that silicon reacted with LiPF_6 .

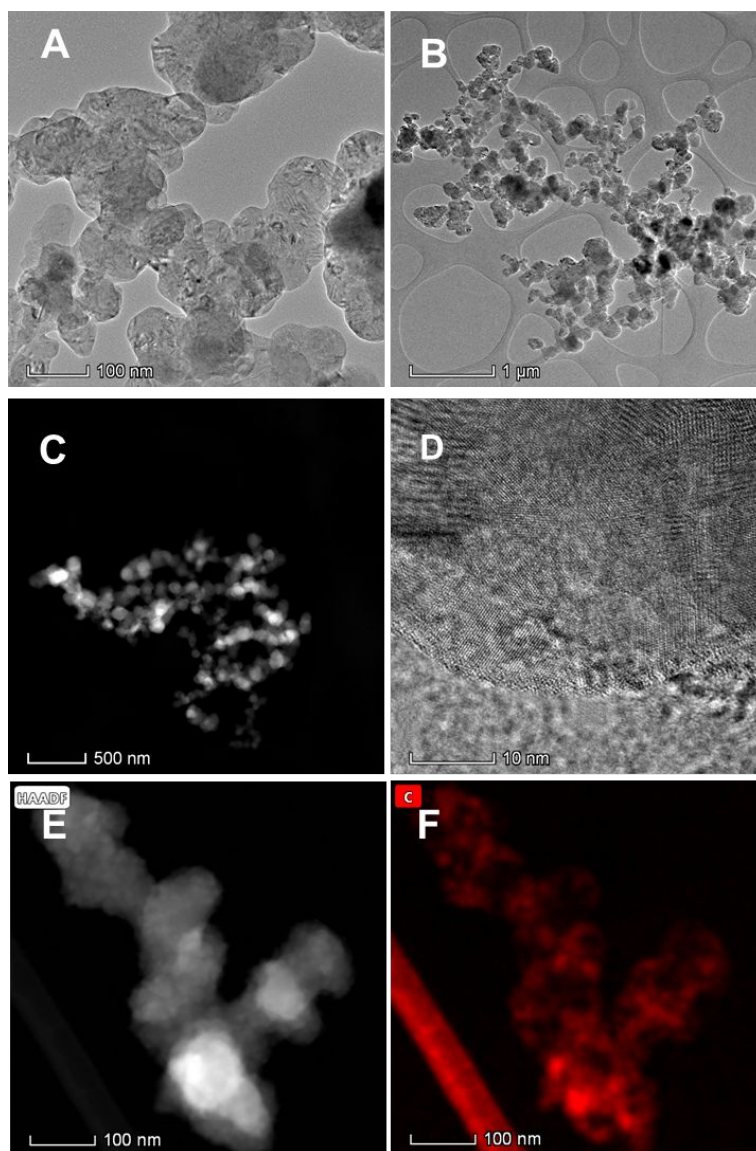


Figure S2. The structure of the Si nanoparticles and Si@C. A) TEM image of the Si nanoparticles; B). Low magnification TEM image of the Si@C nanoparticles; C). Low magnification HAADF image of the Si@C nanoparticles; D) HR-TEM image of Si@C; E) HAADF image of Si@C; F) Corresponding EDS mapping of carbon.

Figure S2A shows a typical low-magnification TEM image of the Si nanoparticles; the Si nanoparticles had a spherical shape with a diameter of approximately 80 nm. Figure S2B, 2C shows Si@C images in a low magnification. The nanoparticles keeps their sphere shape after the carbon coating was added. And the carbon layer could be seen in the HR-TEM image (Figure S2D) of Si@C. Additionally, the lattice fringes of Si could be seen clearly. The HAADF image and the corresponding carbon elemental mapping further proved the existence of carbon on the Si surface.

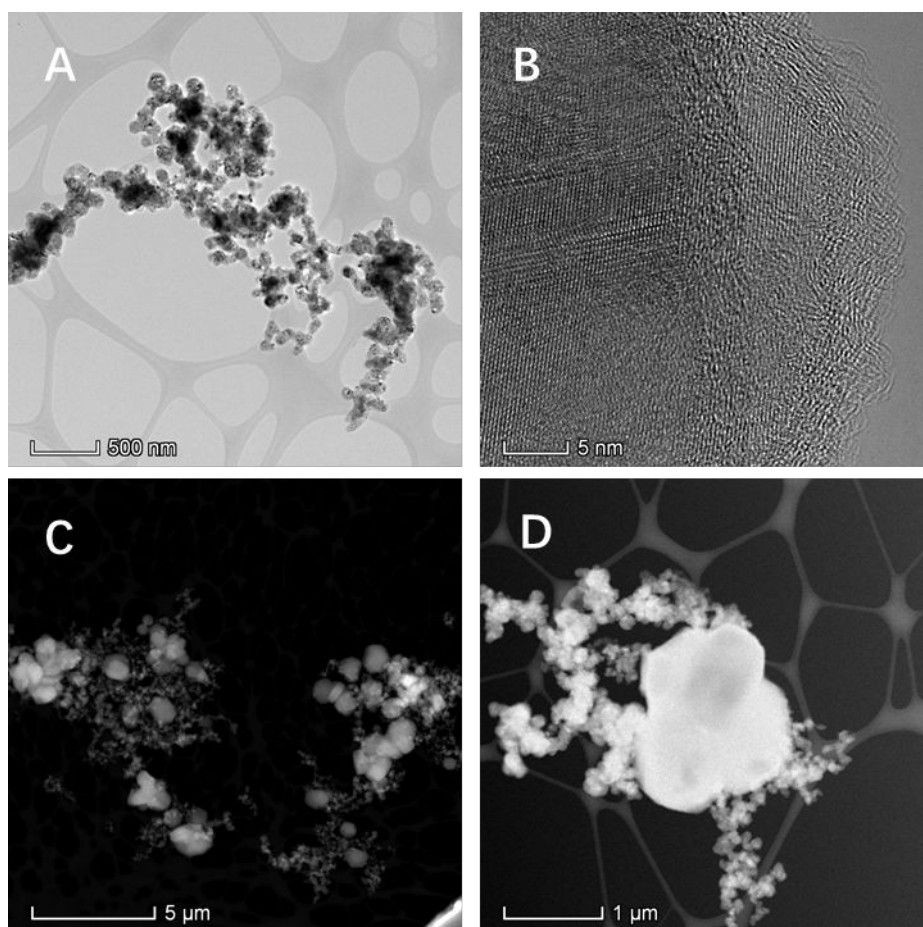


Figure S3. TEM image of Si and Si@C after reacting with electrolyte. A).Low magnification TEM image of Si; B).High resolution TEM image of Si. C, D). Low magnification HAADF image of Si@C.

In a typical low-magnification TEM image of the Si nanoparticles, a small quantity of agglomerations are found. In a HR-TEM image, there is an amorphous layer on the Si surface with the thickness of only 2 nm, which is identified as SiO_x . In the core, the lattice fringe of Si is showed clearly. There is no other amorphous region is found in the TEM image. Figure S3C, 3D shows low magnification HAADF image of Si@C after reacting with electrolyte. In the low magnification, a number of aggregations are found. There are obvious changes huge change between Si and Si@C. Therefore, the results above means that Si cannot react with electrolyte as fast as Si@C.

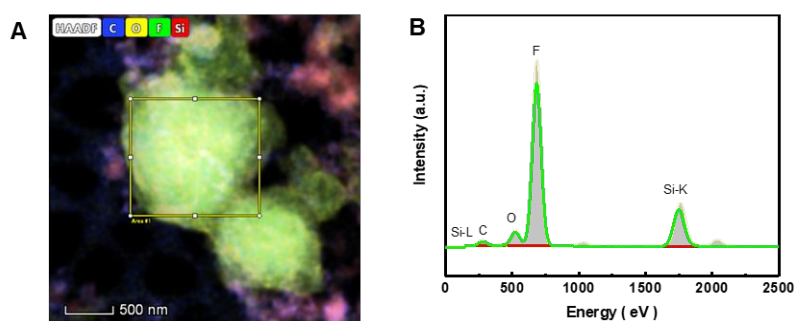


Table S1. The relative content of each element

Element	Atomic Fraction (%)	Atomic Error (%)	Fit error (%)
C	3.70	1.00	1.46
O	6.22	2.09	2.40
F	78.26	26.25	0.92
Si	11.82	3.92	1.77

The merged image (Figure S4A) shows that fluorine was distributed along with silicon and carbon, which further proved that carbon could accelerate the reaction between silicon and LiPF_6 . The specific electron energy spectra of Si and F are shown in Figure S4B. An analysis of the element ratio (Table S1) showed the contents of silicon and oxygen were low, and the main elements were fluorine and silicon. The fluorine/silicon ratio was close to six, revealing that the large clusters mainly consisted of Li_2SiF_6 . The clusters showed that the silicon continuously reacted with LiPF_6 , and the SEI was not able to suppress the reaction. The side reaction is harmful to the performance of the battery and caused the capacity to rapidly decrease due to continuous consumption of silicon, lithium and electrolyte.

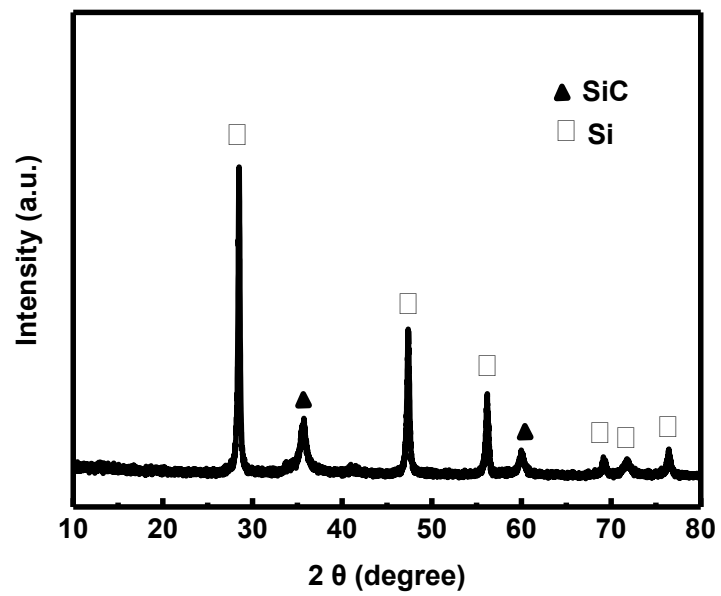


Figure S5. XRD data of Si@SiC@C.

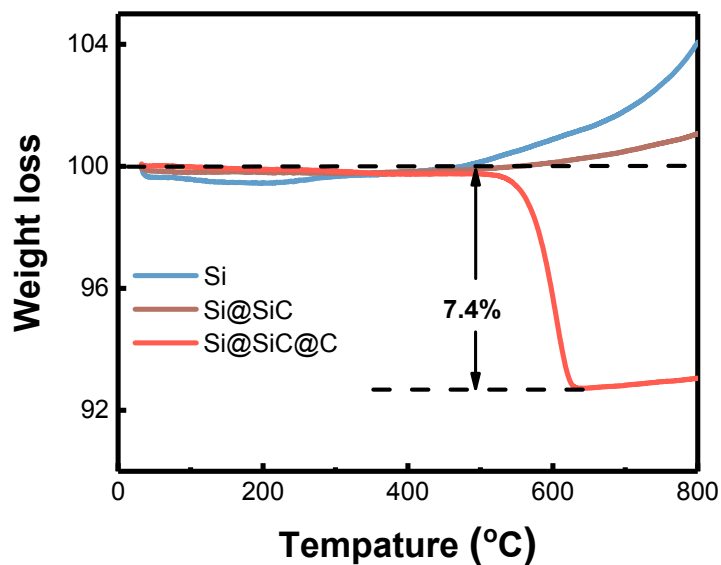


Figure S6. TGA data of Si, Si@SiC, and Si@SiC@C in an oxygen environment.

TGA was performed in an atmosphere of pure O₂ with a flow rate of 50 mL/min, and the heating rate was 10°C min⁻¹. For Si, the weight increment with increasing temperature was due to the reaction of silicon with O₂. For Si@SiC, the weight increment ratio was lower than that for silicon, which proved that the SiC layer could prevent permeation of O₂, suppressing the reaction of silicon with O₂. Based on the TGA data, the integrity of the SiC layer could be analyzed. In addition, the content of the outer carbon shell was 7.4 wt%.

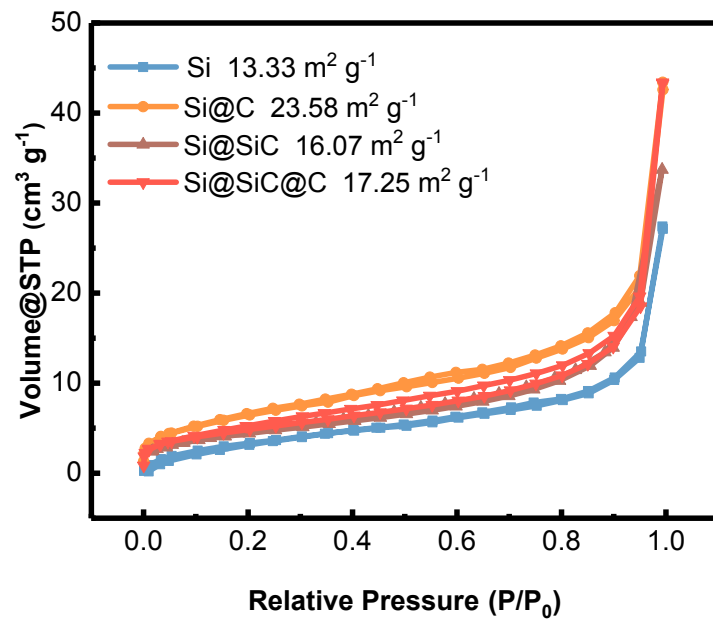


Figure S7. Nitrogen adsorption/desorption isotherm curves of Si, Si@C, Si@SiC, and Si@SiC@C.

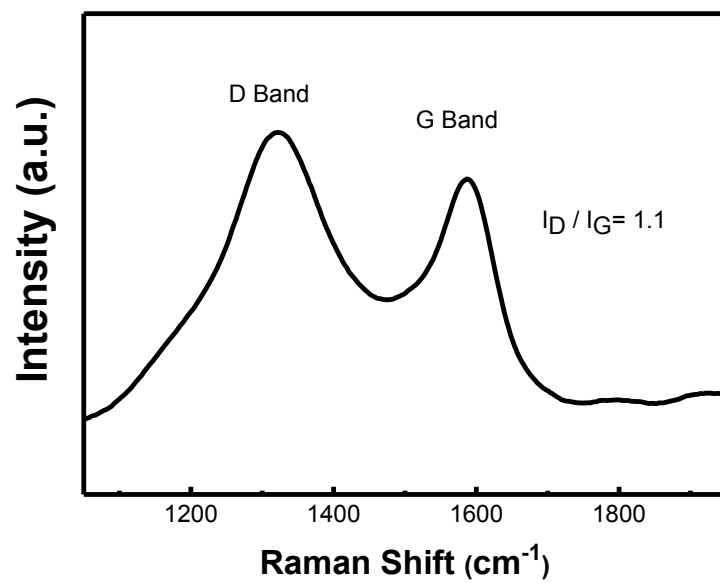


Figure S8. Raman spectra of Si@SiC@C.

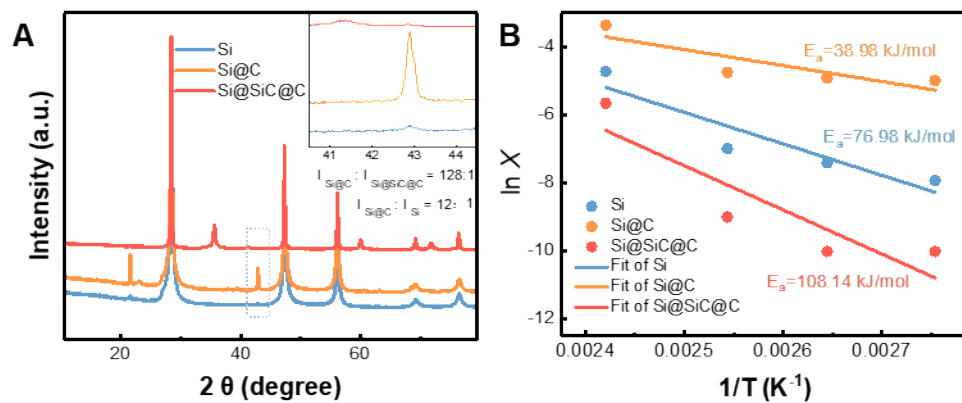


Figure S9. The comparison of Si, Si@C and Si@SiC@C at 90 °C, respectively. A). XRD survey of Si, Si@C and Si@SiC@C after reacting with electrolyte; B). The activation energy for the reactions of Si, Si@C and Si@SiC@C with $LiPF_6$.

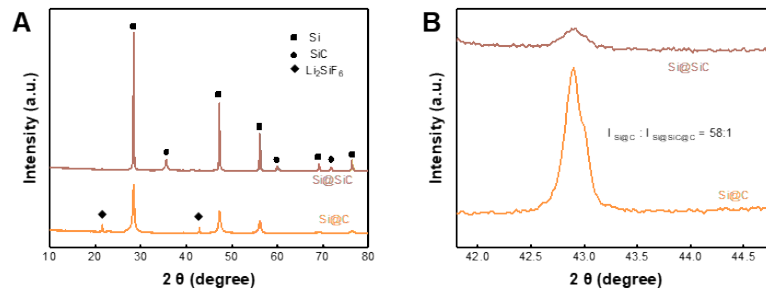


Figure S10. A). XRD survey of Si@C and Si@SiC after the reaction with the electrolyte; B). Partially enlarged drawing.

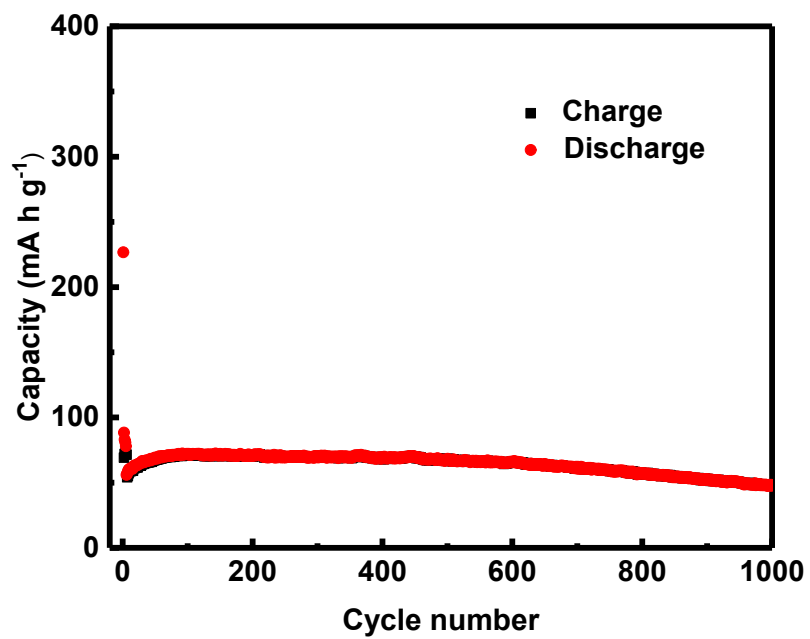


Figure S11. The cycling performance of SiC at a current density of 1 A g⁻¹.

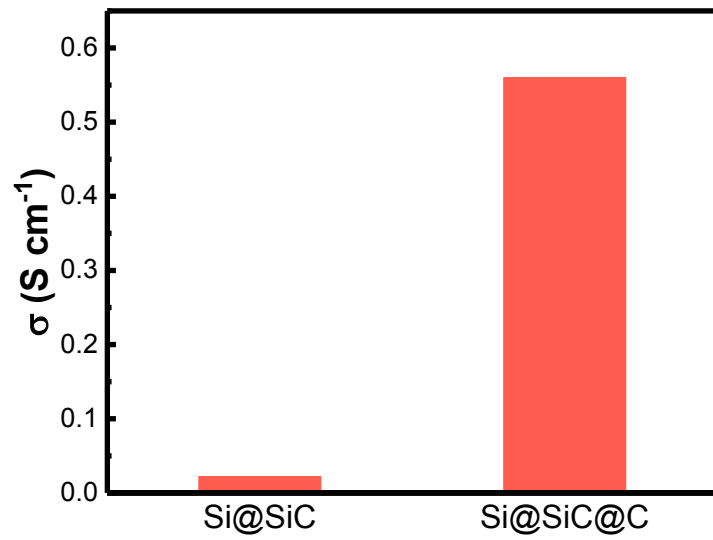


Figure S12. The conductivity of Si@SiC and Si@SiC@C at a pressure of 10 MPa.

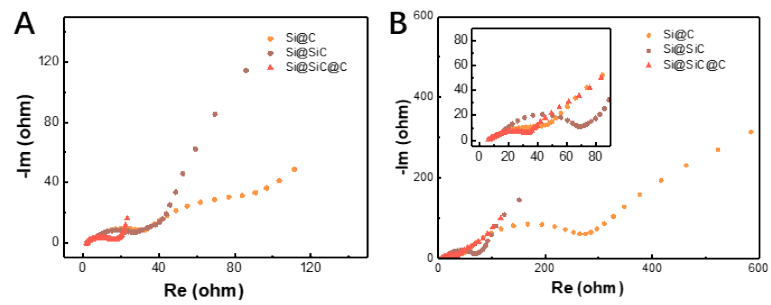


Figure S13. The EIS spectra of Si@C, Si@SiC, and Si@SiC@C. A) After 5 cycles; B) After 100 cycles.

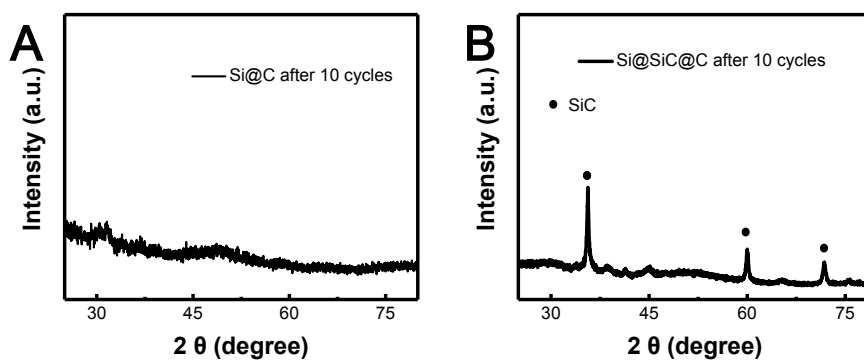


Figure S14. XRD data of different materials after cycling. A). XRD data of Si@C at 2 A g^{-1} after 10 cycles; B). XRD data of Si@SiC@C at 2 A g^{-1} after 10 cycles.

XRD data of different materials were obtained by disassembling the battery after cycling. The XRD data of Si@C (Figure S14A) showed that Si become amorphous after the first cycle. And the peaks of SiC were clearly found after cycling, meaning that the SiC maintained its integrity during the cycling process.

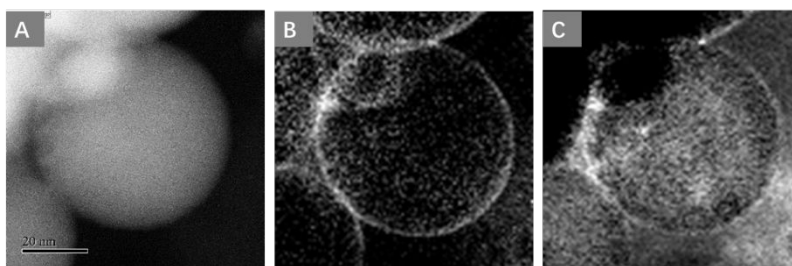


Figure S15. EELS mapping images of Si(A), F (B) and Li (C) for Si@SiC@C after 100 cycles.

The EELS mapping images for Si@SiC@C (Figure S15) were consistent with the EDS mapping images. Fluorine was distributed uniformly on the surface of the silicon in the EELS mapping image (Figure S15B). Moreover, Li was in the inner layer of silicon, and there was a bright boundary on the surface (Figure S15C), showing that Li^+ could easily pass through the SiC layer, which was in agreement with the iDPC-STEM image for SiC after one cycle.